Polymer Journal, Vol. 31, No. 9, pp 739—746 (1999)

Structure Development in a Thermoplastic Polyimide. Cold Crystallization as Revealed by Microhardness

Maria Esperanza CAGIAO, Marco CONNOR,† Francisco Jose BALTÁ CALLEJA,†† and James C. SEFERIS*

Instituto de Estructura de la Materia, CSIC, Serrano119, 28006 Madrid, Spain
**PCL, Department of Chemical Engineering, University of Washington, Box 351750, Seattle, Washington 98195–1750, U.S.A.*

(Received October 1, 1998)

ABSTRACT: The isothermal "cold crystallization" of the thermoplastic polyimide (New TPI) has been studied using the microhardness technique to examine the property-microstructure correlation. By using wide- and small-angle X-ray diffraction and differential scanning calorimetry, the influence of the experimental parameters, *i.e.*, treatment temperature T_c and time t_c on the micromechanical properties of the "cold crystallized" samples has been examined. It is shown that both macroscopic hardness H and volume crystallinity x_c increase with T_c and t_c. For the samples prepared in the secondary crystallization range, it is demonstrated that H values strongly depend on the hardness of the crystalline units H_c. In this range, long spacing L, crystal thickness l_c and crystallinity (both linear x_{CL}, and derived from density x_c) slightly increase with T_c. From the DSC study, it is demonstrated that the proportion of "liquid-like" and "rigid" amorphous fraction present in each sample is directly related with the crystallization conditions. Finally, from the SAXS and DSC combined study, information concerning the secondary crystallization mechanism has been obtained.

KEY WORDS Thermoplastic Polyimide / Microhardness / Crystallinity / "Liquid-Like" and "Rigid" Amorphous Fraction /

Aromatic polyimides have many technological applications, mainly due to their specific chemical structure. The presence of aromatic and imide rings in the monomeric units imparts rigidity to the polymeric chain. As a result, aromatic polyimides exhibit high T_g (glass transition temperature) and T_m (melting temperature) values. Besides good thermal stability, these materials show excellent mechanical and electrical properties and high radiation and solvent resistance. Aromatic polyimides are therefore widely used in specific applications: electronic packaging for printed circuits, insulation for lead wire, etc, being particularly useful in the aerospace industry.

Some specific products of this group, *e.g.*, the so called Kapton (developed by DuPont de Nemours Company) and BTDA-ODA based polyimide (obtained from benzophenone tetracarboxylic dianhydride and 4,4′-oxydianiline) have very rigid chains, being for this reason extremely difficult to melt-process and crystallize. To overcome this inconvenience, synthetic methods have been developed in order to lower the transition temperatures by different routes: incorporation of substitutes in the aromatic rings, introduction of more flexible groups ($(-CH_2-)_n$, –O–) or meta-phenyl linkages into the main chain,[1,2] etc. The thermoplastic polyimide has been synthesized using the last route. Its monomeric unit contains both ether groups and phenyl rings substituted in meta-position.[3]. The result is a crystallizable material with a glass transition temperature T_g of about 250°C. This value is notably lower than those exhibited by other aromatic polyimides. For this reason, the crystallization of New TPI can be easily followed from the molten[3] or from the amorphous solid state ("cold crystallization").[4] The dynamic crystallization of New TPI as it is cooled from the melt can also be easily studied.[5] In all cases, a semicrystalline polymer with a melting point T_m of about 380°C is obtained. This polyimide presents excellent mechanical properties, high-temperature stability, solvent resistance and melt processability.[6,7]

The structure and properties of New TPI have been reported by several research groups.[3–15] Thus, the crystalline structure has been studied by means of the wide-angle X-ray scattering.[8] The spherulitic morphology has been examined by using transmission electron microscopy,[9] and optical microscopy.[3] Other researchers have investigated the rheological[10] and thermal properties[11] of this material. Data concerning the crystal lattice thermal expansion behavior[12] of New TPI have also been reported. Some authors have investigated the stability of this polyimide against radiation,[7,13] whereas others have studied its dielectric and dynamic mechanical relaxation.[14] The crystallization kinetics from the molten state has been investigated by Hsiao, Sauer, and Biswas,[3] and the isothermal cold crystallization kinetics by Huo, Friler, and Cebe.[4] Lu, Cebe, and Capel[15] have used real time small-angle X-ray scattering (SAXS) and thermally stimulated depolarization currents (TSDC) to study the structural characteristics and relaxation behavior of New TPI. In addition, the dynamic crystallization, while cooling from the melt, was modelled by Seferis and Deshpande[5] through the incorporation of induction time considerations into the Avrami kinetics. It was also found that TPI experiences a loss of "crystallizability" after exposure to multiple processing cycles or extended times at temperatures above the melt. This was attributed to loss of nucleation sites.[5]

The aim of the present study is to extend the above

† Permanent address: *EMS-Chemie AG, CH-7013 Domat/Ems, Switzerland.*
†† To whom correspondence should be addressed.

investigation to examine the structure–microhardness correlation of New TPI. Due to its simplicity, the microhardness technique has become a widely used method for measuring the mechanical properties of polymers.[16-20]. Furthermore, the microhardness is a property sensitive to morphological and structural changes in polymers.[18,19] In particular, the microhardness of glassy polymers has been shown to be affected by the changes occurring in the morphology as a result of the crystallization from the glassy state.[21,22] Hence, we think that the microhardness could be applied to the study of the structure development of New TPI after crystallization using calorimetric and X-ray scattering methods.

This work forms part of a wider research project directed to clarify the crystallization mechanism underlying the higher-order structures of crystalline polymers.[23]

EXPERIMENTAL

New TPI polyimide has been developed by Mitsui Chemical Co. (formerly Mitsui Toatsu Chemical Co.). The samples used in this study were transparent, amorphous, 80 and 200 μm thick films. The amorphous samples were "cold crystallized" by annealing them at the temperatures and times indicated in Table I. The thermal treatment was carried out in a Linkam heating device. It is noteworthy that no other treatment was performed on the films before the "cold crystallization" process.

Density was measured at 23°C by a density gradient column filled with a carbon tetrachloride-*n*-hexane mixture. Volume crystallinity values x_c were derived from the density ρ data by using the expression:

$$x_c = (\rho - \rho_a)/(\rho_c - \rho_a) \quad (1)$$

assuming for the density of the crystals a value $\rho_c = 1.467\,g\,cm^{-3}$ [8] and for the amorphous density a value $\rho_a = 1.328\,g\,cm^{-3}$ (calculated in this work).

Wide-angle X-ray scattering (WAXS) patterns were obtained in the reflection mode using a Rigaku-Denki goniometer. A rotating anode X-ray generator using Ni-filtered Cu-K_α radiation working at 40 KV and 140 mA was used. The SAXS patterns were obtained with a point collimation Rigaku camera (sample to film distance = 300 mm) and, in some cases, with a point collimation Kiessig camera (sample to film distance = 500 mm). Ni-filtered Cu-K_α radiation from a 40 kV, 70 mA source was used. The long spacings (L) were obtained from the SAXS patterns by directly applying the Bragg's law to the diffraction maxima of the various samples.

The samples were analyzed by differential scanning calorimetry (DSC) using a Perkin-Elmer DSC 7 model. The sample weight was 3.5—5 mg, being the heating rate 20°C min^{-1}. All scans were performed in a N_2 atmosphere.

Microhardness (H) was measured at room temperature using a Leitz tester adapted with a square-based diamond indenter with included angles α between non adjacent faces of the pyramid of 136°. The H value was derived from the residual projected area of indentation according to the expresion $H = kP/d^2$ (MPa), where d is the length of the impression diagonal in meters, P is the contact load applied in N and k is a geometrical factor equal to 1.854. A loading cycle of 0.1 min and loads of 0.15, 0.25, and 1 N were used. Preliminary hardness measurements were performed at the surface and in the interior of the samples. It was found that the surface layer of the TPI samples was harder than the bulk (see Figure 1). In what follows, we shall refer our results to microhardness measurements performed on the samples surface.

Table I. Preparation conditions of New TPI samples

T_c / °C	270	280	310	320	330						
t_c / min	0	3	5	10	15	30	45	60	90	120	180

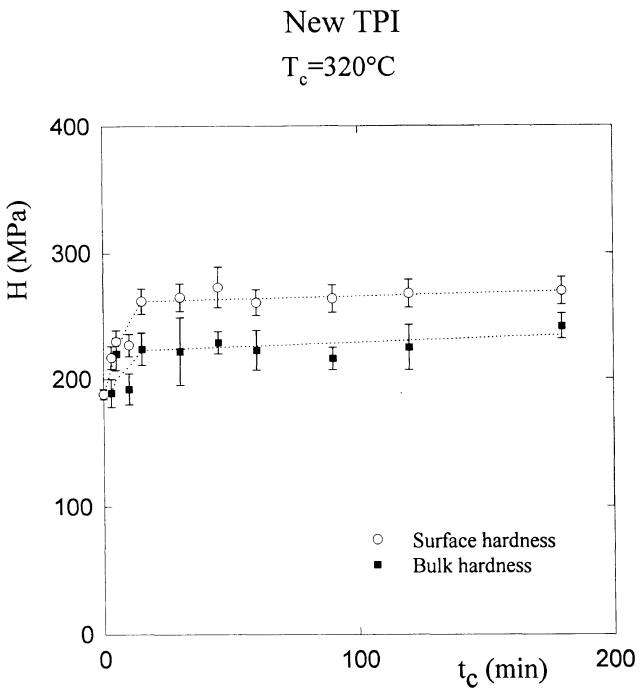

Figure 1. Surface (open symbols) and bulk (filled symbols) microhardness as a function of crystallization time t_c for samples of New TPI "cold crystallized" at $T_c = 320$°C.

RESULTS

Microhardness Studies

The studied samples were crystallized from the glassy state for different times at different temperatures (see Table I). To discuss the results obtained we shall distinguish between two morphologies: i) Structures obtained by interrupting the primary crystallization (the growth of spherulites is not completed), ii) Structures in which the growth of spherulites is completed, obtained by crystallization at different temperatures beyond the end of the primary crystallization.

Figure 2 shows the initial gradual increase (from an initial value $H_a = 185$ MPa, corresponding to the amorphous TPI) and the final leveling off in H as a function of the crystallization time t_c for the various tem-

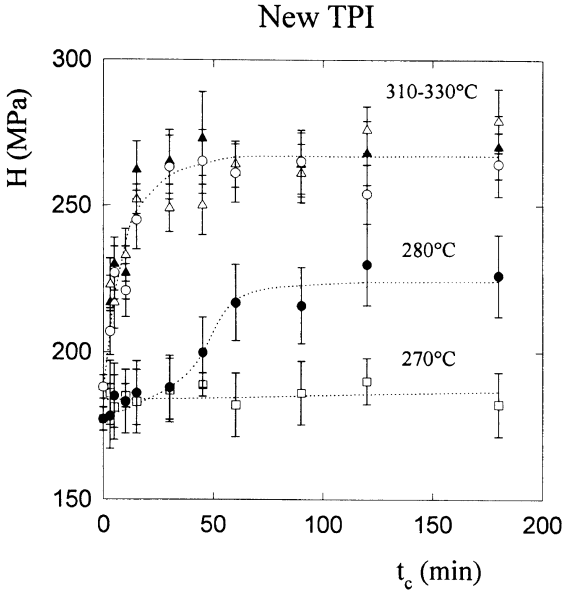

Figure 2. Surface hardness *vs.* crystallization time t_c of New TPI "cold crystallized" for various crystallization temperatures T_c.

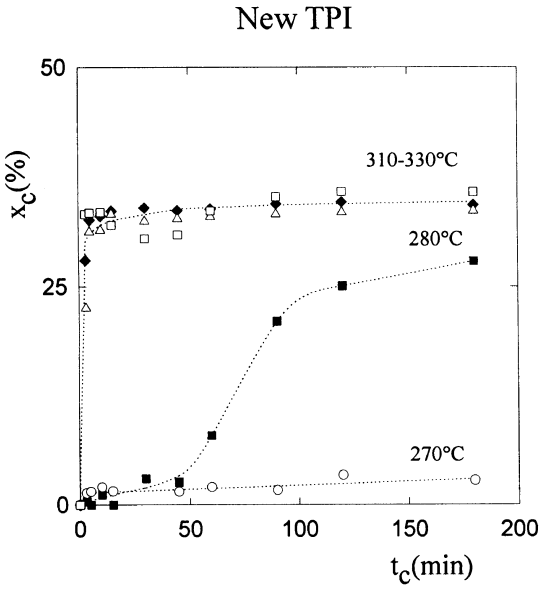

Figure 3. Degree of crystallinity x_c (derived from density) of New TPI "cold crystallized" at various temperatures T_c as a function of the crystallization time t_c.

peratures T_c.

In order to obtain samples in which the growth of spherulites is not completed, we have crystallized amorphous New TPI at 270 and 280°C for different times. At $T_c = 270$°C the hardening process is very slow with a negligible H variation. However, the H increase for $T_c = 280$°C shows two well defined regions: a first faster raise until $t_c \cong 60$ min, and then a much slower H increase up to values of 220 MPa for $t_c \cong 180$ min. In the range $T_c = 310$—330°C, the hardness increases very quickly until $t_c = 15$ min and then it levels off to final values between 264 and 279 MPa. We have represented the H–t_c variation for the three highest temperatures by a unique curve for the sake of clarity. The hardness increase observed for each crystallization temperature is correlated with the development of crystallinity as shown in

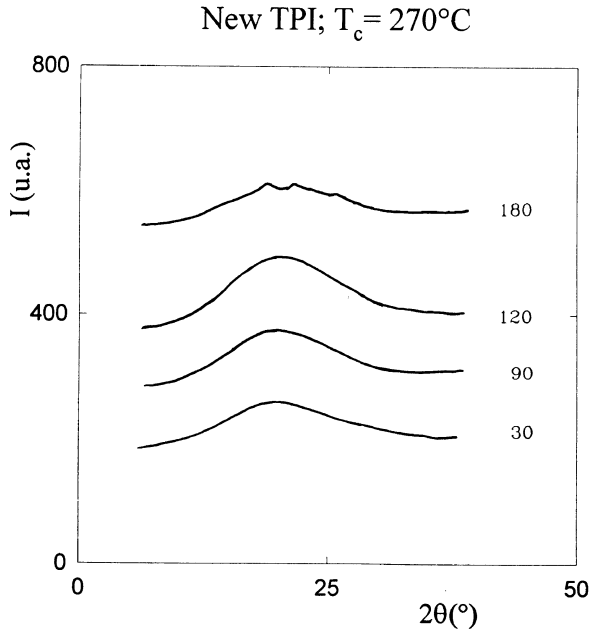

(a)

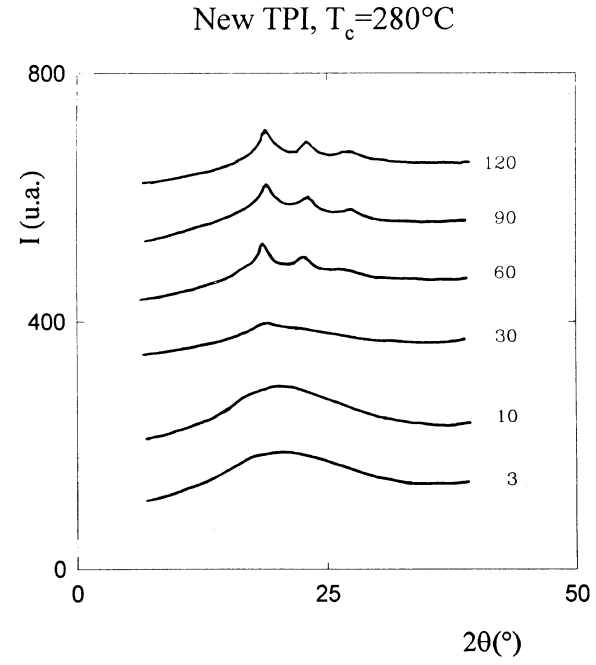

(b)

Figure 4. Evolution of the WAXS diagrams for New TPI samples crystallized at (a) 270°C and (b) 280°C during different crystallization times t_c. Beside each diagram, t_c in minutes is indicated.

Figure 3. Here the degree of crystallinity x_c determined from density is plotted as a function of time for various temperatures. As it can be seen, x_c values of 33—36% are reached at the end of the crystallization for the higher temperatures. It is noteworthy that for the almost negligible increase in H at $T_c = 270$°C (Figure 2) a very small crystallinity value $x_c \cong 3\%$ is observed.

Figure 4 illustrates the structure evolution as a function of time for $T_c = 270$ and 280°C respectively by WAXS. In the case of the samples crystallized at $T_c = 270$°C, the appearance of very faint crystalline reflexions is observed only for $t_c \geq 180$ min (Figure 4a). At $T_c = 280$°C the crystalline reflections start appearing for $t_c \geq 30$ min

Table II. Crystallinity values obtained from density data, x_c, and from WAXS, x_c^{RX}, in New TPI samples "cold crystallized" at $T_c = 330°C$

t_c/min	x_c/%	x_c^{RX}/%
15	32.0	21.7
60	33.6	22.1
90	35.2	23.6
120	35.8	24.3
180	35.8	23.3

Table III. Crystalline fraction, x_c, "liquid-like" amorphous fraction x_a, and "rigid" amorphous fraction x_{ra} in New TPI samples crystallized at different temperatures T_c

T_c/°C	x_c[a]	x_a[a]	x_{ra}[a]	x_c[b]	x_a[b]	x_{ra}[b]
310	0.31	0.40	0.29	0.24	0.61	0.15
320	0.33	0.38	0.29	0.25	0.62	0.13
330	0.34	0.38	0.28	0.26	0.62	0.12

[a] This work; $t_c = 10$ min. [b] Huo, Friler, and Cebe[4]; $t_c = 10$ min.

Table IV. Long spacing, L, crystal thickness, l_c, and amorphous phase thickness, $L-l_c$ evolution with crystallization time t_c in New TPI samples "cold crystallized" at $T_c = 310$, 320, and 330°C

t_c/min	310°C			320°C			330°C		
	L/Å	l_c/Å	$L-l_c$/Å	L/Å	l_c/Å	$L-l_c$/Å	L/Å	l_c/Å	$L-l_c$/Å
3	206	76	130	213	99	114	214	114	100
5	209	105	104	208	107	101	212	109	103
10	203	105	98	207	110	97	210	112	98
120	195	101	94	204	110	94	212	117	95

(Figure 4b). For the samples crystallized at $T_c \geq 310°C$ the crystalline peaks appear immediately.

The crystallinity values obtained from WAXS were calculated by dividing the area of the crystalline peaks by the total diffracted area, and are ~30% lower than those derived from density data. Table II illustrates comparatively both sets of values for New TPI samples crystallized at 330°C. One possible explanation for this difference has been discussed in terms of the role played by the interface located at the lamellar surface.[14,15,24]

Calorimetry and Microstructure (Rigid Amorphous Fraction)

From the DSC study, the heat-capacity increment ΔC_p at T_g for each sample was measured, and from these data the "liquid-like" amorphous fraction, x_a, and "rigid" amorphous fraction, x_{ra}, values have been derived. The mobile or "liquid-like" amorphous fraction is defined as the fraction of the amorphous phase that undergoes a distinct heat-capacity jump at T_g, similar to the one observed with purely amorphous sample.[4] The value of x_a is defined as:

$$x_a = \Delta C_p / \Delta C_p^a \quad (2)$$

where ΔC_p^a is the heat-capacity increment of a 100% amorphous sample. The "rigid" amorphous fraction, x_{ra}, is originated by the constraint of crystal lamellae on amorphous chains in the semicrystalline samples.[4] The x_{ra} value is derived from[25,4]:

$$x_{ra} = 1 - x_c - x_a \quad (3)$$

Table III illustrates the comparison between the x_c, x_a, and x_{ra} values found in this work, and those reported by Huo, Friler, and Cebe.[4] It is important to note that these researchers have obtained the x_c, x_a, and x_{ra} data from the calorimetric study, and used $\Delta H_m^\infty = 139$ J g^{-1} [4,25] as the heat of fusion of a 100% crystalline sample to calculate the x_c fraction. However, our x_c values have been obtained from density data. Both series of values are considerably different, particularly those of x_a and x_{ra} fractions. This is probably due to the fact that our samples have been only subjected to a "cold crystallization" process, whereas the samples studied by Huo *et al.*[4] were previously dried (150°C, 20 h), and finally relaxed (260°C, 20 h). Therefore, a possible explanation for this discrepancy could be the lower molecular mobility in our samples as compared to those studied by Huo *et al.*

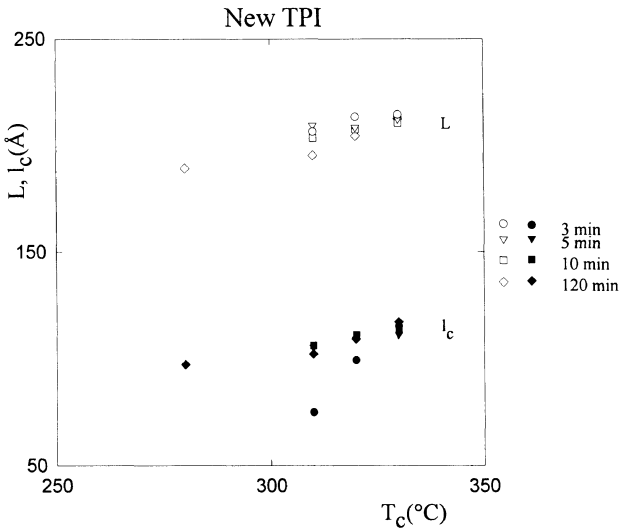

Figure 5. Long spacing L (open symbols) and average crystal thickness l_c (filled symbols) derived from SAXS and DSC for New TPI samples "cold crystallized" for different times t_c, as functions of crystallization temperature T_c.

For a given temperature, the long spacing L slowly decreases as a function of treatment time t_c (see Table IV). The crystal thickness l_c, derived from

$$l_c = x_c L / (1 - x_a) \quad (4)$$

increases very quickly during the first 5 min and then levels off. Table IV shows the L and l_c evolution with t_c for the samples crystallized at 310, 320, and 330°C. Figure 5 shows the variation of both long spacing L and crystal thickness l_c with the crystallization temperature T_c. The thickness, $L-l_c$, of the amorphous phase is nearly

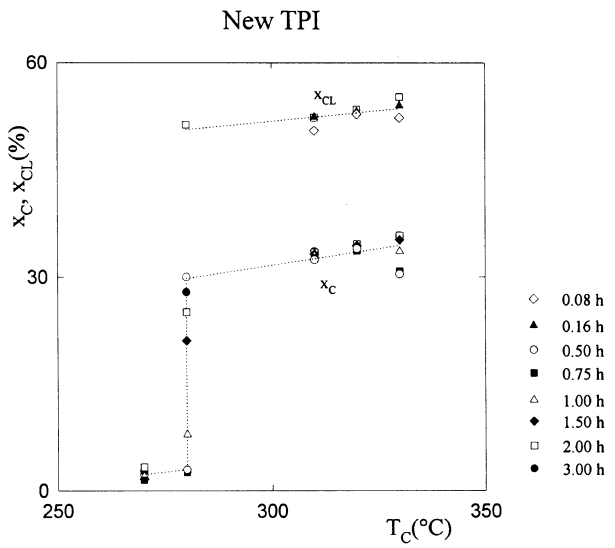

Figure 6. Linear crystallinity $x_{CL}=l_c/L$, derived from SAXS and DSC, and crystallinity x_c derived from density, for New TPI samples isothermally crystallized from the glassy state for different times t_c as a function of T_c.

Table V. Thermal properties of New TPI samples "cold crystallized" at $T_c=320°C$ for different times t_c

t_c	T_g	ΔC_p	x_a	T_m	ΔH_m
min	°C	J g K^{-1}	%	°C	J g^{-1}
3	245.3	0.12	40	325.2 382.5	37.50
5	244.3	0.12	38	323.7 382.6	38.45
10	245.8	0.12	38	327.7 382.8	39.11
120	245.3	0.11	35	330.4 381.8	41.51

T_g and T_m, glass transition and melting temperatures; ΔC_p, heat-capacity increment at T_g; x_a, "liquid-like" amorphous fraction derived from the ΔC_p data (see the text); ΔH_m, total melting enthalpy calculated for both T_{m1} and T_{m2} peaks.

independent of T_c for long treatment times t_c (see Table IV).

In Figure 6 it can be seen that both the volume crystallinity, x_c, (see eq 1) and the linear crystallinity, x_{CL}, defined as:

$$x_{CL}=l_c/L \tag{5}$$

show a similar dependence on T_c.

The DSC heating scans of most isothermally crystallized specimens exhibit two distinct maxima T_{m1} and T_{m2}. The former value T_{m1} occurred from 3 to 13 degrees above T_c and the latter, T_{m2}, was nearly independent of t_c and T_c. Table V lists the calorimetric data of samples crystallized at $T_c=320°C$, being ΔH_m the total melting enthalpy calculated for both peaks, T_{m1} and T_{m2}. This double melting behavior can be explained by the reorganization model. The first melting peak comes from the crystals present in the sample at room temperature, before the scan takes place. These crystals are very imperfect, and melt just above the cold crystallization temperature, giving rise to the first peak at T_{m1}. After a recrystallization reorganization process,

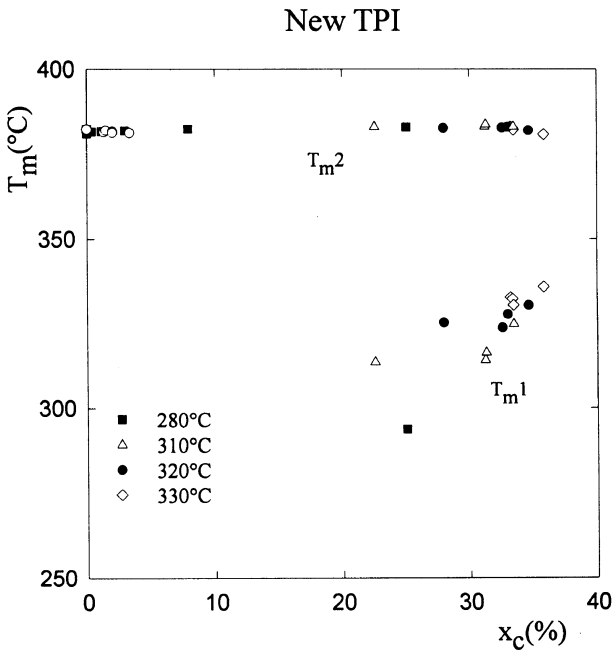

Figure 7. Plot of the upper T_{m2} and lower T_{m1} melting peak temperature as a function of the crystallinity degree x_c (derived from density), for New TPI samples isothermally crystallized from the glassy state at different temperatures T_c and for different times t_c.

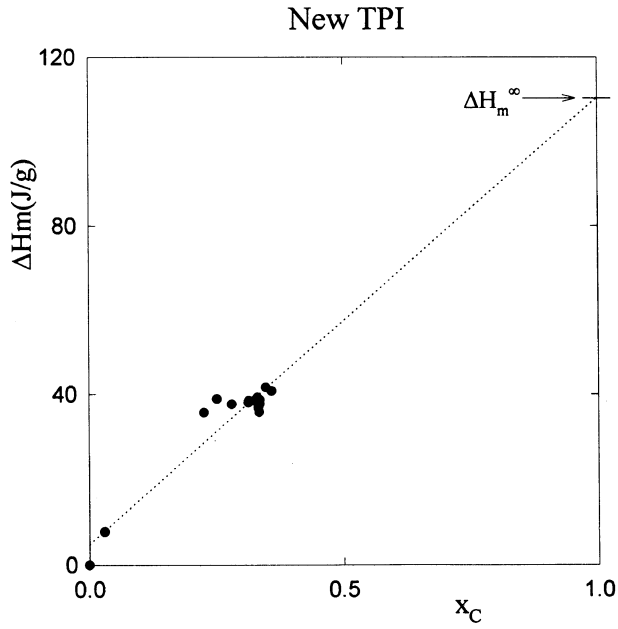

Figure 8. Heat of fusion ΔH_m as a function of density ρ for New TPI "cold crystallized" at different temperatures T_c and for different times t_c.

they eventually melt again at T_{m2}.[4] It can be clearly seen in Figure 7 that T_{m1} increases with x_c, whereas T_{m2} remains practically constant. This result, together with the L and l_c variation with t_c (see Table IV) favors the crystal insertion model, *i.e.*, secondary crystalline structures grow between the primary lamellae as crystallization proceeds.[3]

The linear relationship between the heat of fusion ΔH_m and the crystallinity x_c, for samples crystallized at different temperatures for different times (Figure 8), after extrapolation to $x_c=1$, yields for the heat of fusion of a 100% crystalline sample, $\Delta H_m^\infty=110$ J g^{-1}. This value is

Table VI. New TPI samples "cold crystallized" at $T_c = 310$, 320, and 330°C for different times t_c

t_c/min	310°C		320°C		330°C	
	x_c	x_c^{DSC}	x_c	x_c^{DSC}	x_c	x_c^{DSC}
3	22.6	32.3	28.0	34.1	33.2	33.3
5	31.2	34.4	32.6	35.0	33.4	32.4
10	31.3	34.8	33.0	35.6	33.5	35.0
120	33.5	34.2	34.6	37.7	35.8	36.9

Comparison between x_c, crystallinity derived from density data, and x_c^{DSC}, crystallinity obtained from the calorimetric study, using the value $\Delta H_m^\infty = 110\,J\,g^{-1}$ as the melting enthalpy for a 100% crystalline sample (see the text).

Table VII. Surface free energy, σ_e, calculated for New TPI samples "cold crystallized" at $T_c = 310$, 320, and 330°C for different times t_c

t_c/min	σ_e/erg cm^{-2}		
	310°C	320°C	330°C
3	36	48	55
5	50	52	53
10	50	53	55
120	48	53	59

lower than the one reported by Mitsui Toatsu,[26] $\Delta H_m^\infty = 139\,J\,g^{-1}$, and in fair agreement with the data of Hsiao, Sauer, and Biswas,[3] $\Delta H_m^\infty = 116\,J\,g^{-1}$, and Deshpande and Seferis,[27] $\Delta H_m^\infty = 112.5\,J\,g^{-1}$. The crystallinity values x_c^{DSC} calculated from the melting enthalpy data by using our value $\Delta H_m^\infty = 110\,J\,g^{-1}$ are very similar to the volume crystallinity data x_c derived from density measurements (see Table VI for comparison). Only in the samples treated at 310 and 320°C for 3 min a discrepancy between x_c and x_c^{DSC} values can be found, probably due to the crystallization of the material upon heating of the DSC. Therefore, we consider our ΔH_m^∞ value to be correct. As it was above indicated, T_{m2} is almost constant and does not depend on the crystal thickness l_c, as it was previously demonstrated by Hsiao, Sauer, and Biswas for samples crystallized at $T_c \leq 320$°C.[3] Therefore, if σ_e is defined as the surface free energy, the Thomson–Gibbs equation:

$$T_m = T_m^0[1 - (2\sigma_e/\Delta H_m^\infty l_c)] \quad (6)$$

cannot be applied to derive the T_m^0 value (equilibrium melting temperature) from T_m and l_c data. Thus, the value $T_m^0 = 424$°K obtained by Lu *et al.*[15] was used in eq 6 together with the value of $\Delta H_m^\infty = 110\,J\,g^{-1}$ obtained in this study in order to calculate the surface free energy σ_e. In this way σ_e values varying between 36 and 59 erg cm^{-2} were derived (see Table VII). These values are higher than the one reported by Lu, Cebe, and Capel, $\sigma_e = 41$ erg cm^{-2}.[15] During the first 3—5 min, σ_e slightly increases, and then levels off. The highest σ_e values are obtained for the highest crystallization temperature $T_c = 330$°C.

DISCUSSION

In the course of isothermal crystallization at and above

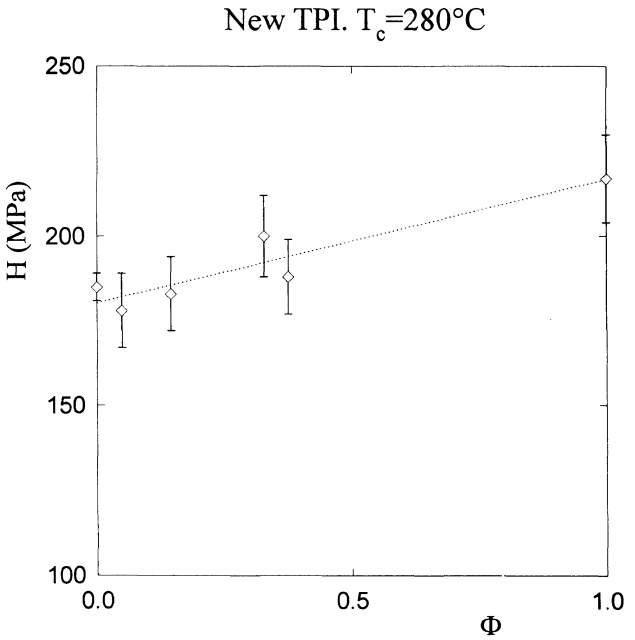

Figure 9. Plot of the macroscopic hardness H as a function of the volume fraction of spherulites, $\Phi = \alpha/\alpha_0$.

$T_c = 280$°C one observes first a rapid sigmoidal increase of the degree of crystallinity x_c, followed by a very slow raise (Figure 3). The first rapid increase is associated to primary crystallization. The following much slower process is called secondary crystallization.[28] During primary crystallization one often observes spherulites growing until they impinge to each other.[28]

It is noteworthy that the variation of H during isothermal crystallization also shows the first rapid increase (Figure 2). However, in the region of secondary crystallization H remains constant. This behavior is similar to that exhibited by poly(ethylene terephthalate) (PET) "cold crystallized" from the glassy amorphous state at $T_c > 120$°C.[21] The cause for this discrepancy between H and x_c in the secondary crystallization regime has to be sought in the mechanical behavior of the rigid amorphous regions constrained between the crystal lamellae. Let us assume that the yield process (microhardness) in the rigid amorphous regions is the same as in the crystalline lamellae. Then, after primary crystallization, when the spherulites fill up the samples completely, the H value remains constant while the crystallinity increases due to the gradual crystallization of the amorphous interlamellar regions.

In the primary crystallization region the growth of spherulites is not completed and the expresion[21]:

$$H = H_{sph}\Phi + H_a(1 - \Phi) \quad (7)$$

can be used to calculate the hardness of the spherulitic material. In the above expresion H_a is the hardnesss of the amorphous glassy material and $\Phi = \alpha/\alpha_0$[21] is the volume fraction of the spherulites, being α the crystallinity value after a time t_c and α_0 the crystallinity at which H levels off when the primary crystallization process is completed. Figure 9 shows the variation of H as a function of Φ for $T_c = 280$°C. We have found that H_{sph} varies between 215 and 230 MPa, increasing with T_c.

In the second region (secondary crystallization) the

Table VIII. Crystalline phase hardness, H_c, and b (measure of the hardness depression from ΔH_c^∞, see the text), calculated for New TPI samples "cold crystallized" at $T_c = 310$, 320, and 330°C for different times t_c

t_c/min	H_c/MPa			b/Å
	310°C	320°C	330°C	
10	251	260	271	94
120	334	339	348	46

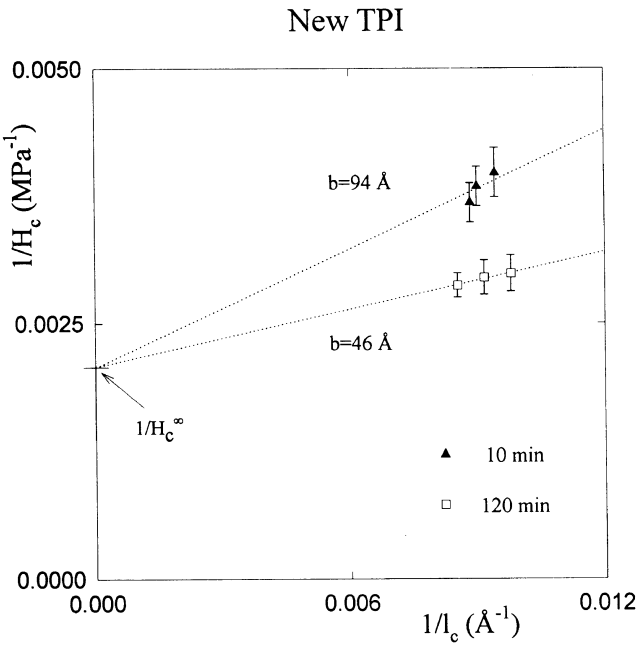

Figure 10. Plot of the reciprocal crystal hardness $1/H_c$ against the reciprocal crystal thickness $1/l_c$ for "cold crystallized" New TPI at $T_c = 310$—330°C.

hardness additivity law for semicrystalline polymers[29]:

$$H_{sph} = H_c x_{CL} + H_a(1 - x_{CL}) \quad (8)$$

applies. $x_{CL} = l_c/L$ is the linear crystallinity, as it was above defined. H_c and H_a are the hardness values for the crystalline and amorphous phase respectively. In this way, the hardness of the crystal lamellae H_c for each sample was derived (see Table VIII). It is also known that the relationship between H_c and l_c is given by[30]:

$$H_c = H_c^\infty/(1 + b/l_c) \quad (9)$$

Figure 10 shows the plot $1/H_c$ *versus* $1/l_c$ for $t_c = 10$ and 120 min. In this plot, b/H_c^∞ represents the slope of each straight line. H_c^∞ is the hardness of an infinitely large crystal. The b parameter is a measure of the hardness depression from H_c^∞, and is equal to $2\sigma_e/\Delta h$,[31] where σ_e is the surface free energy of the crystal lamellae and Δh is the energy for crystal destruction. The b value was found to decrease from 94 to 46 Å when t_c increases from 10 to 120 min (Figure 10 and Table VIII). From the analysis of the results obtained in the characterization of the samples, it can be seen that, for samples prepared in the secondary crystallization range, the crystal thickness l_c increases only slightly with T_c and t_c (Table IV and Figure 5), and so does the linear crystallinity x_{CL} (Figure 6). These variations are not sufficient to explain the macroscopic hardness H increase with both T_c and t_c. Contrary to the "cold crystallized" PET samples above cited,[21] in Table VIII it can be clearly seen that in the TPI samples presented in this study the crystalline hardness H_c is strongly dependent on the treatment temperature and time. From these results, one can conclude that for semicrystalline New TPI "cold crystallized" samples, the macroscopic hardness H depends mainly on the crystalline hardness H_c, the latter being an increasing function of T_c and t_c. The H_c increase with t_c could be explained by the decrease of the b parameter from 94 to 46 Å in going from $t_c = 10$ min to $t_c = 120$ min (see Figure 10 and Table VIII). As the surface free energy σ_e is almost constant for each temperature, the b behavior could be related to the increasing perfection or higher degree of order of the crystals with t_c, thus giving rise to higher values of the Δh (energy for crystal destruction) as t_c increases.

CONCLUSIONS

- Cold crystallization of New TPI above 310°C yields a material with H values near 270 MPa. This is one of the largest hardness values obtained for synthetic rigid polymers.
- From the microhardness study it seems clear that macroscopic hardness H is strongly influenced by the hardness of the crystalline units H_c, which is an increasing function of treatment temperature T_c and time t_c.
- Data concerning the crystalline, "liquid-like" amorphous and "rigid" amorphous fraction have also been derived. From the evolution of the long spacing and crystal thickness during the thermal treatment, and from the melting behavior, we have concluded on the existence of secondary crystalline structures between the primary lamellae.

Acknowledgments. The authors are indebted to DGICYT (Grant PB94-0049), Madrid (Spain). We wish also to thank NEDO's International Joint Research Programme, Japan, for the generous support of this investigation. Partial financial support was provided by the Polymeric Composites Laboratory Consortium at the University of Washington.

REFERENCES

1. C. Arnold, *Macromol. Rev., J. Polym. Sci.*, **14**, 265 (1979).
2. P. M. Hergenrother and S. J. Havens, *J. Polym. Sci.*, **27**, 1161 (1989).
3. B. S. Hsiao, B. B. Sauer, and A. Biswas, *J. Polym. Sci., Part B, Polym. Phys.*, **32**, 737 (1994).
4. P. P. Huo, J. B. Friler, and P. Cebe, *Polymer*, **34**, 4387 (1993).
5. A. Deshpande, Doctoral Dissertation, University of Washington (1996).
6. J. B. Friler and P. Cebe, *Polym. Eng. Sci.*, **33**, 587 (1993).
7. T. Sasuga, *Polymer*, **32**, 1539 (1991).
8. K. Okuyama, H. Sakaitani, and H. Arikawa, *Macromolecules*, **25**, 7261 (1992).
9. T. Takahashi, S. Yuasa, M. Tsuji, and K. Sakurai, *J. Macromol. Sci., Phys.*, **B33**, 63 (1994).
10. T. H. Hou and R. M. Reddy, *SAMPE Q.*, **22**, 38 (1991).
11. M. V. Brillhart and P. Cebe, *J. Polym. Sci., Part B, Polym. Phys.*, **33**, 927 (1995).

12. S. X. Lu, P. Cebe, and M. Capel, *Polymer*, **37**, 2999 (1996).
13. T. Hirade, Y. Hama, T. Sasuga, and T. Seguchi, *Polymer*, **32**, 2499 (1991).
14. P. P. Huo and P. Cebe, *Polymer*, **34**, 696 (1993).
15. S. X. Lu, P. Cebe, and M. Capel, *J. Appl. Polym. Sci.*, **57**, 1359 (1995).
16. B. Darlix, B. Monasse, and P. Montmitonnet, *Polym. Test.*, **6**, 107 (1986).
17. R. J. Ion, M. Pollock, and C. Roques-Cames, *J. Mater. Sci.*, **25**, 1444 (1990).
18. Y. Deslandes, E. Alva Rosa, E. Brisse, and T. Meneghini, *J. Mater. Sci.*, **26**, 2769 (1991).
19. F. J. Baltá Calleja, *Trends Polym. Sci.*, **2**, 419 (1994).
20. F. J. Baltá Calleja, and S. Fakirov, *Trends Polym. Sci.*, **5**, 246 (1997).
21. C. Santa Cruz, F. J. Baltá Calleja, H. G. Zachmann, N. Stribeck, and T. Asano, *J. Polym. Sci., Part B, Polym. Phys.*, **29**, 819 (1991).
22. D. R. Rueda, A. Viksne, L. Malers, and F. J. Baltá Calleja, *Macromol. Chem. Phys.*, **195**, 3869 (1994).
23. Proc. NEDO International Symposium on Polymer Crystallization: "Fundamental Studies on Crystallization of Polymers," Kyoto, March 1998.
24. U. Köncke, H.G. Zachmann, and F. J. Baltá Calleja, *Macromolecules*, **29**, 6019 (1996).
25. P. P. Huo and P. Cebe, *Macromolecules*, **25**, 902 (1992).
26. Technical Data Sheet A-00, Mitsui Toatsu Chem., Inc., Tokyo, Japan.
27. A. P. Deshpande and J. C. Seferis, *J. Thermoplastic Compos. Mat.*, submitted.
28. H. G. Zachmann and C. Wutz, in "Crystallization of Polymers," NATO ASI Series, M. Dosier, Ed., Kluwer Acad. Publishers, Dordrecht, 1993, p 403.
29. F. J. Baltá Calleja, J. Martinez de Salazar, and D. R. Rueda, *Encycl. Polym. Sci. Eng.*, **7**, 614 (1987).
30. F. J. Baltá Calleja, and H. G. Kilian, *Coll. Polym. Sci.*, **266**, 29 (1988).
31. F. J. Baltá Calleja, C. Santa Cruz, R. Bayer, and H. G. Kilian, *Coll. Polym. Sci.*, **268**, 440 (1990).